EOS

EOS, TRANSACTIONS, AMERICAN GEOPHYSICAL UNION

VOLUME 86 NUMBER 6

8 FEBRUARY 2005

PAGES 57–64

Global Seismographic Network Records the Great Sumatra-Andaman Earthquake

PAGES 57, 60–61

On 26 December 2004 the Indonesian subduction zone near the northern end of Sumatra began to rupture at 58 minutes, 47 seconds past midnight Greenwich Mean Time. The rupture continued for approximately seven minutes, extending northwestward along the Sunda Trench for roughly 1200 km to the Andaman Islands. The seafloor displacement generated a massive tsunami that swept ashore with 10-m amplitude in northern Sumatra and expanded across the Indian Ocean and Andaman Sea, striking Sri Lanka and Thailand within two hours of the rupture. Confirmed deaths along the coastlines of 11 Indian Ocean nations exceed 220,000, marking this as one of the most lethal natural disasters in human history.

The 2004 Sumatra-Andaman earthquake is the largest event since the 1964 Good Friday Alaskan earthquake ($M_w = 9.2$), releasing approximately as much strain energy as all global earthquakes between 1976 and 1990 combined. Displacement occurred across the shallow-dipping thrust fault and may have exceeded 20 m in some areas, totaling to a moment magnitude (M_w) of 9.0 (seismic moment of $M_0 = 4.0 \times 10^{22}$ N-m). This is the first earthquake of this size to occur since the advent of digital seismometry. Its moment release is eight times that of the previous largest event, the great Peru earthquake of 23 June 2001 ($M_w = 8.4$).

As the fault ruptured, it radiated seismic waves into the surrounding rock. The elastic waves expanded outward through Earth's interior as *P* and *S* waves and along its surface as Love and Rayleigh waves. These waves sounded alarms at the Pacific Tsunami Warning Center in Hawaii as they were recorded by telemetered seismographic stations worldwide. The ground began to shake in Sri Lanka when the first *P* wave arrived 4 minutes after the onset of rupture. After 12 minutes, *P* waves had reached Europe and Antarctica. Every position on Earth's surface began to vibrate within 21 minutes. And such vibrations they were! The ground shaking was detected by thousands of seismometers worldwide, but sensors of extraordinary bandwidth and dynamic range were needed to capture this giant earthquake fully. Fortunately, many such stations have been deployed in the past few decades.

The Global Seismographic Network (GSN) is funded by the U.S. National Science Foundation (NSF) in partnership with the U.S. Geological Survey (USGS), and operated by the Incorporated Research Institutions for Seismology (IRIS), the USGS, the University of California, San Diego, and a number of cooperating institutions [*Butler et al.*, 2004]. The GSN now includes 137 high dynamic range, broadband seismic stations around the world, deployed as a multi-use facility for global monitoring of earthquakes and nuclear explosions and scientific investigations of earthquakes and Earth structure.

All GSN data are open and freely available through the IRIS Data Management Center (http://www.iris.edu). Most stations have real-time telemetry through various global communication circuits including Internet and satellite communications. An original design goal for the GSN was to deploy instrumentation that would record with high fidelity all seismic motions for earthquakes anywhere in the world with magnitudes as large as 9.0. The Sumatra-Andaman earthquake was the first full-scale test of the GSN, and the network performed well (Figure 1).

From the nearest GSN stations with real-time telemetry (PALK on Sri Lanka and COCO in the Cocos-Keeling Islands) to those near the event's antipode (OTAV in Ecuador), on-scale recordings of the strongest motions produced by the earthquake were obtained along with the tiny motions associated with subsequent oscillations of our entire planet. The peak-to-peak ground shaking for Rayleigh waves arriving at PALK was 9.2 cm. Even at the most remote distances, the ground moved up and down more than 1 cm as R_1 swept across Earth's surface. Such records are unprecedented; all stations of the former World Wide Standardized Seismic Network were driven off-scale for hours by the 1964 Alaskan earthquake due to the limitations of 1960's seismographic technology.

The Sumatra-Andaman earthquake was felt throughout southeastern Asia. At greater distances, the largest-amplitude vibrations were too slow for human perception; nevertheless, all of Earth's creatures rode this motion as the main seismic surface waves flexed the surface.

Seismic signals like those in Figure 1 enable robust determination of the earthquake rupture processes, and form the basis for most of what could be determined quickly about its faulting. With continuous telemetry of signals from the global GSN stations, a variety of near- real-time processing procedures are enabled for all earthquakes.

This includes automatic event detection from the first-arriving seismic waves by earthquake monitoring operations such as those of the USGS National Earthquake Information Center and the NOAA Pacific Tsunami Warning Center. Both of these operations rely extensively on real-time GSN data for initial reporting of global earthquakes. Once an event is located, the recorded vibrations allow seismic magnitude estimation and inversion for fault orientation and slip direction. Rapid quantification of the earthquake source is useful for tsunami warning and emergency response.

Unfortunately, ocean pressure sensors are not yet available in the Indian Ocean or Andaman Sea to complement seismic analysis procedures, and effective communications and public warning systems to reach coastal areas are yet lacking. Thus, the full advantage of rapid analysis of seismic data could not be realized for this event.

Due to the long rupture duration for the event, every seismic phase has a correspondingly prolonged duration. The *P* wave energy continued to arrive for minutes, and this is true for all subsequent seismic phases such as *PP*, *S*, *ScS*, etc. Figure 2 compares the Sumatra-Andaman seismogram with a recording of the 17 January 1994 Northridge earthquake (M_w = 6.7) that caused more than 50 deaths and more than $30 billion in property damage in Southern California. The greater magnitude of the Sumatra-Andaman event is reflected in both the larger amplitude and the vastly longer rupture process. Discrete pulses in the Northridge seismogram correspond to the distinct body wave arrivals *P*, *PP*, and *PPP*. The *PP* and *PPP* phases arrive during the prolonged *P* arrival from the Sumatra-Andaman earthquake, so the rupture process cannot be isolated within a single body wave phase. The high-pass-filtered

By J. Park, K. Anderson, R. Aster, R. Butler, T. Lay, and D. Simpson

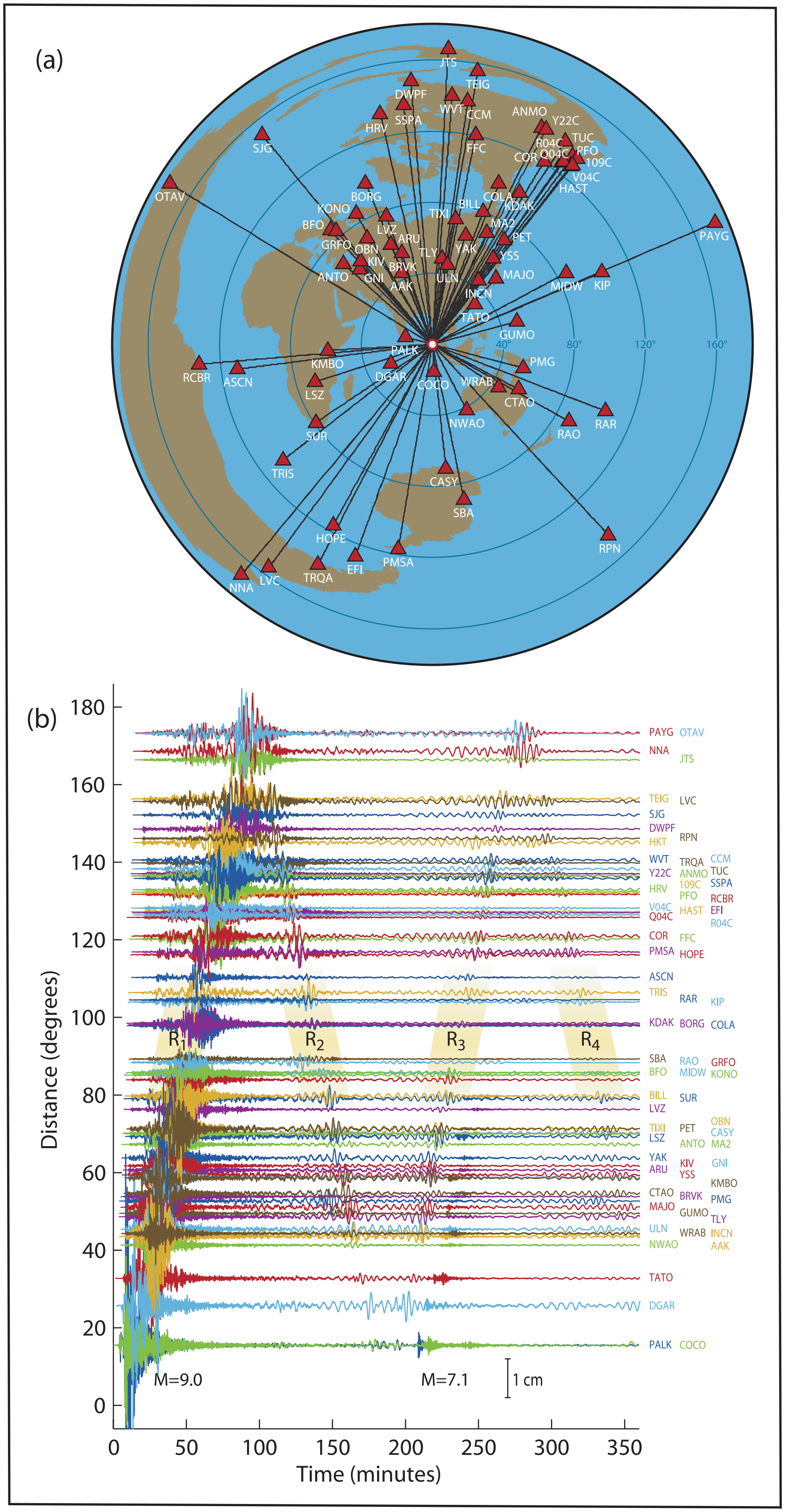

Fig. 1. (a) Map of station locations for the Global Seismographic Network with real-time or near-real-time data availability from the Sumatra-Andaman earthquake, showing distance in degrees. (b) Six hours of vertical ground shaking for the Sumatra-Andaman earthquake at GSN stations worldwide displayed against distance from the source. The ground motions are dominated by surface waves (Rayleigh waves), which produced peak-to-peak amplitudes of over 1 cm (see scale at lower right) everywhere on Earth's surface. The series of major arrivals at each station involve R_1 (Rayleigh wave that travels along the minor great circle arc), R_2 (Rayleigh wave traveling along the major great circle arc), R_3 (the same pulse as R_1, but with an additional global circuit), and R_4 (the same pulse as R_2 with an additional global circuit). Signals for a large (M_w = 7.1) aftershock are visible at the closest stations at a time delay of about 200 min.

version of the *P* wave (Figure 2) de-emphasizes secondary surface reflections and suggests ~400 s of primary rupture.

The Sumatra-Andaman earthquake ruptured with strong directionality, piling up energy toward the northwest from the event epicenter. Rupture directionality is critical for earthquake and tsunami hazard. If rupture had progressed southeast along the Indonesian plate boundary rather than northwest, Banda Aceh and Thailand's beaches might have been spared devastation, but heavy damage would have been expected along the southern Sumatran coast.

P wave timing determines the epicenter, i.e., where rupture starts. Other observations determine rupture directivity from stations aligned with and against the strike of the earthquake fault. These include Doppler shifts in amplitude and frequency content, and station-by-station variations in apparent rupture duration. Computer algorithms can determine the direction of rupture in a rapid and robust manner from the details of *P* wave signals. Analyses of the first 200 s of *P* wave motion at GSN stations by many researchers have already yielded slip models for the portion of rupture near Sumatra. All models detect northwest rupture progression and slip patches with ~20 m of underthrusting motion. Preliminary studies of broadband surface waves suggest a total duration of rupture of 360 s.

While the integration of geodetic, tsunami, and other constraints will establish details of the earthquake more firmly, rapid analysis of GSN data provided first-order features of the event and its aftershock sequence. Source-rupture modeling would be a useful augmentation to existing tsunami hazard assessment procedures.

Surface wave signals sweep around the world repeatedly after a large earthquake (see R_1 to R_4 in Figure 1), forming interference patterns that comprise standing waves, or normal vibrational modes, within Earth. Effectively, the 2004 Sumatra-Andaman earthquake rang our planet like a bell at very long periods, exciting a multitude of normal mode vibrations. Spectral analysis of GSN recordings detects these modes, further constraining the overall characteristics of the earthquake (Figure 3).

The longest-period mode $_0S_2$ (54 min) deforms Earth's surface in a pattern that resembles a football. Preliminary estimates suggest that the earthquake raised this vibration to an average height of more than 0.1 mm worldwide. Internal friction within Earth causes the $_0S_2$ vibration to lose amplitude by roughly 0.5% in each oscillation cycle, so it should disappear into background noise a few weeks after the earthquake.

By contrast, the "breathing vibration" $_0S_0$ (period 20.5 min), in which Earth expands radially outward and then contracts inward, loses amplitude by only 0.05% in each oscillation cycle. The Sumatra-Andaman quake raised $_0S_0$ to an initial amplitude of roughly 0.06 mm. This vibration of the entire planet should remain detectable in seismic data well into April 2005.

The initial phase of $_0S_0$ estimates the midpoint of the earthquake rupture process, relative to the initial breakage of the fault. Initial $_0S_0$ phase values of 60–65° (Figure 3) suggest that the halfway point for the Sumatra-Andaman rupture occurred more than 200–225 s after it began, implying a total rupture time of 400–450 s (~7 min), roughly consistent with other estimates.

Geophysicists will make scientific discoveries based on the GSN recordings of this earthquake for some time (preliminary results are being posted at http://www.iris.iris.edu/sumatra). Societal benefits will accrue from a better understanding of tsunami generation, finite fault rupture, and total fault motions involved in this event. Some scientific questions can be addressed only with an earthquake of this magnitude. Geophysicists will search for large aseismic strain pulses in the seismic and geodetic data from this event. This may aid our understanding of recent observations of (largely) aseismic strain release in the Cascadia subduction zone in the Pacific Northwest [*Rogers and Dragert*, 2003], a plate boundary which suffered its own $M_w \geq 9$ rupture on 26 January 1700 [*Satake et al.*, 1996].

Geophysical research depends on data. The GSN network has now demonstrated the capability to record on-scale ground motions worldwide from earthquakes as large as the 26 December 2004 Sumatra-Andaman event. Technological advances have enabled real-time data acquisition and rapid response capabilities that were not fully envisioned when IRIS, NSF, and the USGS designed the GSN in 1984.

Yet, the capabilities of the system have not been exploited fully. Expanded tsunami warning capabilities for many regions of the world could build upon the GSN and comparable-quality stations of the Federation of Digital Seismic Networks (FDSN). Improved station coverage and telemetry would enhance the current system.

The terrible damage and loss of life wrought by this earthquake humble the most dispassionate observer, as does the strong likelihood that one or more $M_w \geq 9$ earthquakes will

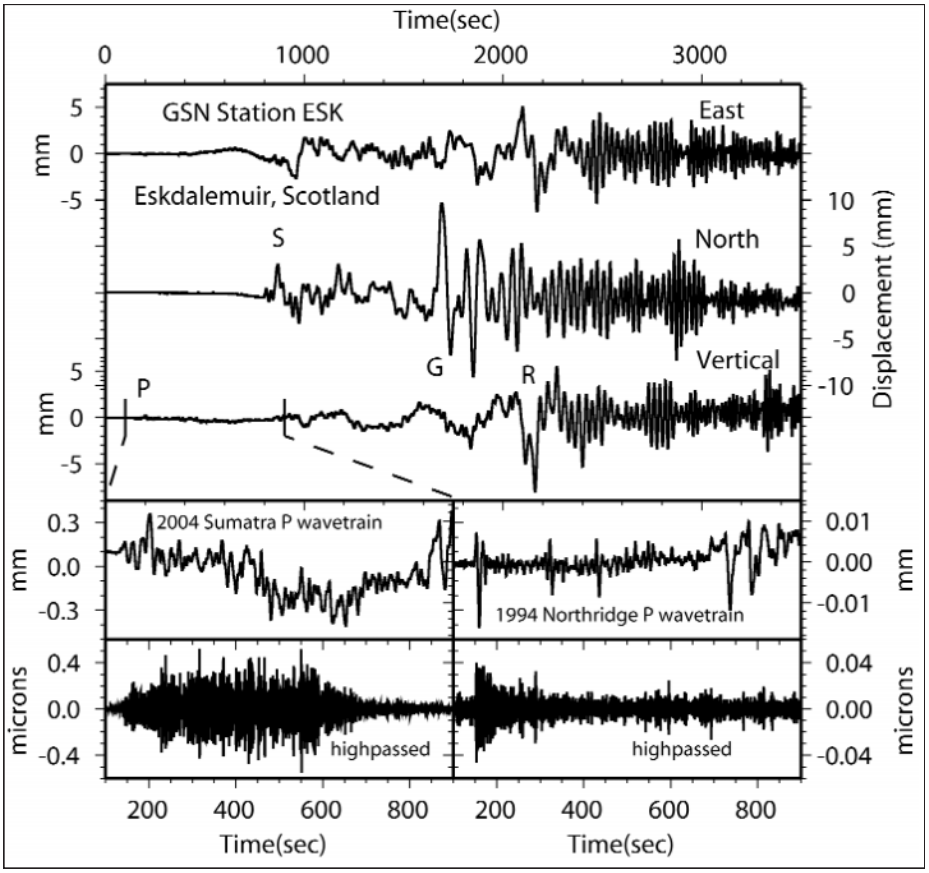

Fig. 2. Ground motions recorded by GSN station ESK in Scotland. Three-component ground shaking for the 2004 Sumatra-Andaman earthquake is shown at the top. The largest motions are the Love (G) and Rayleigh (R) surface waves which moved the ground by about 1 cm. Displacements associated with the P *(pressure) and* S *(shear) body waves, which travel through Earth's deep interior, ranged from 0.1 to several millimeters. The lower panels compare the* P *wave ground motion at ESK with that for the 17 January 1994 Northridge earthquake* ($M_w = 6.7$)*. Note the different vertical scales. The 2004 ground motions dwarf the 1994 motions in both amplitude and duration. The bottom panels show* P *wave motions for both events filtered to contain only frequencies greater than 1 Hz, which emphasizes direct waves radiating from the primary fault rupture. The greatly extended duration of the 2004 event is clear.*

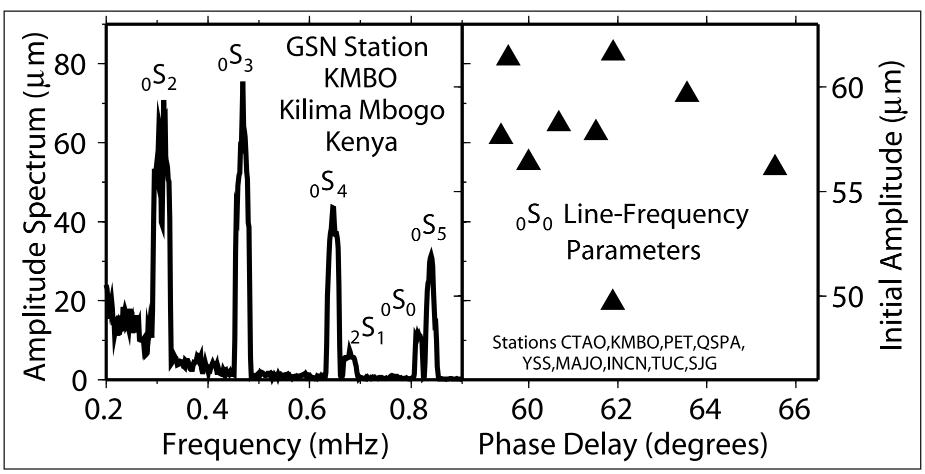

Fig. 3. (left) Amplitude spectrum based on 96 hours of vertical ground motion at GSN station KMBO in Kenya. Peaks in the spectrum indicate normal modes of Earth excited by the earthquake. Several spectral peaks corresponding to known Earth free vibrational modes are labeled. The clear peak at the lowest frequency is $_0S_2$*, which involves football-shaped fluctuations in Earth shape. The small peak at 0.8146 mHz (20.5-min oscillation period) is* $_0S_0$*. This involves radial expansion and contraction of Earth. The Sumatran quake raised these free vibrations to amplitudes almost 10 times larger than ever before measured with modern digital seismometers. (right) Estimates of amplitude and initial phase angle for* $_0S_0$ *at nine different GSN stations. The initial phase of* $_0S_0$ *can be used to estimate that the midpoint of the earthquake rupture process is 200–225 s after it began. This suggests that the total rupture continued for approximately 7 min.*

occur elsewhere in the coming century. Sustained operation of the GSN will ensure that ground motion recordings are available for scientific analysis and emergency response applications.

Acknowledgments

Data are provided by the IRIS/USGS Global Seismographic Network (GSN) and distributed through the IRIS Data Management System. GSN stations are operated by the U.S. Geological Survey's Albuquerque Seismological Laboratory, the University of California, San Diego, and affiliate partners. Local station hosts contribute to GSN operations, many GSN sites are joint stations with FDSN partners (Australia, Canada, China, France, Germany, Italy, Japan, Mexico, New Zealand, Russia), and telemetry of GSN data involves multiple facilities and collaborations, including the U.S. National Weather Service and the Comprehensive Test Ban Treaty Organization. This article demonstrates the importance of these collaborative efforts. Support for these networks is provided by NSF and USGS. The facilities of the IRIS Consortium are supported by NSF under Cooperative Agreement EAR-0004370.

References

Butler, R., et al. (2004), The Global Seismographic Network surpasses its design goal, *Eos Trans. AGU, 85*(23), 225.

Rogers, G., and H. Dragert (2003), Episodic tremor and slip on the Cascadia subduction zone: The chatter of silent slip, *Science, 300*, 1942–1943.

Satake, K., K. Shimazaki, Y. Tsuji, and K. Ueda (1996), Time and size of a giant earthquake in Cascadia inferred from Japanese tsunami records of January 1700, *Nature, 379*, 246–249.

Author Information

Jeffrey Park, Yale University, New Haven, Conn.; Kent Anderson, IRIS Consortium, Washington, D.C.; Richard Aster, New Mexico Institute of Mining and Technology, Socorro; Rhett Butler, IRIS Consortium, Washington, D.C.; Thorne Lay, University of California, Santa Cruz; and David Simpson, IRIS Consortium, Washington, D.C.

For additional information, contact J. Park; E-mail: jeffrey.park@yale.edu.

MEETINGS

Salt Marsh Geomorphology: Physical and Ecological Effects on Landform

PAGES 57–58

Salt marshes are among the most productive ecosystems on the planet, producing more organic matter per unit area than forests, grasslands, and cultivated fields. Marsh landscapes typically fringe low-energy coastal environments, but in places they may extend inland tens to hundreds of kilometers.

As a consequence of their high productivity and interactions with the coastal ocean, salt marshes provide numerous benefits to society. For example, salt marshes are critical habitats for commercially harvested marine and estuarine biota; they filter nutrients and sediment from the water column; and they provide recreational opportunities. In addition, salt marshes help dissipate erosive tide and wave energy, and they have intrinsic aesthetic values. All of these societal benefits have a quantifiable economic value, and salt marsh impairment and degradation have associated costs.

The high productivity and resulting societal benefits of salt marshes are sustained by recurrent interactions between physical and biological processes. These processes operate within the context of human modification of the landscape, including changes imparted to mechanical and biological energy flows (e.g., land use).

In the last two centuries, coastal urbanization has destroyed extensive areas of salt marsh, forcing a dependence on the few remaining salt marsh ecosystems to maintain key ecosystem functions, such as organic matter production and the interception and transformation of terrestrial nutrients.

Likewise, salt marsh processes continue to function under a regime of eustatic sea level rise. As a consequence, some of the extant salt marsh landscapes are subject to greater instability, whereas new salt marsh areas are likely to develop in different coastal locations. Hence these unique and biologically essential landscapes are subject to degradation, transformation, and regeneration in response to natural and anthropogenic forcing.

A recent Chapman Conference entitled "Salt Marsh Geomorphology: Physical and Ecological Effects on Landform," organized by AGU, focused on the integration of physical and ecological sciences to enhance understanding of the interactions between salt marsh geomorphology and intertidal sedimentary processes (see the conference Web site at http://www.geol.sc.edu/chapman/index.htm, and the Bay of Fundy photos at http://www.gly.fsu.edu/~fagherazzi/halifax/index.htm).

The major scientific goals of the conference were (1) to present a comprehensive synthesis on the feedbacks between salt marsh ecology and geomorphology; (2) to determine research questions of key importance for the coupling of ecological and geomorphological processes in salt marshes; and (3) to develop a common language that can be used by scientists from different disciplines to exchange information.

Scientists from North America, Europe, Asia, and Australia attended the meeting along with consultants involved in salt marsh restoration projects around the world.

Biosedimentary and Biogeochemical Processes

The influence of biophysical processes on sediment transport is a key component of the ecomorphological evolution of salt marshes. For example, the vegetation canopy modifies marsh hydrodynamics, thus enhancing sediment deposition and erosion on the marsh platform. Benthic mats and biological films also modify the physical characteristics of sediments, considerably increasing resistance to erosion. Furthermore, microbial assemblages enhance sediment capture and retention among the marsh plants.

Conference presentations underlined the complexity of biosedimentary processes and the future research needs in this area. Similarly, biogeochemical processes and nutrient cycling have an important role in controlling plant development, with evident consequences for landscape evolution. New approaches linking biogeochemical processes to marsh morphology and plant distribution were outlined in the conference. For example, it has been proven that the most rapid rates of carbon and nitrogen cycling are observed in sediments vegetated by the tall form of *Spartina alterniflora* near the creek banks.

Coupled Biological and Morphological Models of Salt Marsh Evolution

A session of the conference was devoted to conceptual and quantitative models of salt marsh evolution. Coupled biological and physical models are only recently coming to light, and enable a comprehensive description and quantification of salt marsh interactions. It was clear from the conference that numerical models rely on the description of physical and biological processes by mathematical relationships parameterized with field investigations and laboratory experiments.

Given the novelty of this research field, some expressions utilized in the models still need scientific testing. For example, still lacking is a quantitative relationship for below-ground organic production and the processes that control it. Despite this limitation, numerical models of salt marsh evolution are highly effective at describing the complex interactions between biota and sediment transport processes, and can drive field investigations on specific processes fundamental for the co-evolution of the salt marsh landscape.

The conference session also stressed the importance of a precise characterization of equilibrium states in salt marshes. In fact, the final goal of the modeling approach is the determination of the rates at which the coupled biological and physical system moves toward equilibrium or switches between two different equilibrium configurations.